

# Thermo-mechanical factors influencing annealing twin development in nickel during recrystallization

Y. Jin<sup>1</sup> · B. Lin<sup>2</sup> · A. D. Rollett<sup>2</sup> · G. S. Rohrer<sup>2</sup> · M. Bernacki<sup>1</sup> · N. Bozzolo<sup>1</sup>

Received: 2 February 2015 / Accepted: 28 April 2015 / Published online: 6 May 2015  
© Springer Science+Business Media New York 2015

**Abstract** The effects of prior stored energy level, annealing temperature, heating velocity, and initial grain size on annealing twin development during static recrystallization of commercially pure nickel (99.999 %) are investigated. The twin content (measured as the twin boundary density or as the number of twins per grain) at the end of recrystallization is shown to be primarily influenced by the prior stored energy level and by the initial grain size, but the effects of heating rate and the annealing temperature are negligible. Taken together, the results are consistent with a new proposition that roughness of the recrystallization front promotes the formation of annealing twins during recrystallization.

## Introduction

Grain boundary engineering (GBE), first proposed by Watanabe in 1984 [1], aims at improving intergranular damage resistance by maximizing the fraction of special boundaries in the grain boundary network. Annealing twin boundaries, both coherent and incoherent twin boundaries, are fundamental for GBE [2, 3]. Despite the fact that these twin boundaries are well known from the beginnings of

physical metallurgy [4], the understanding of annealing twin formation mechanism remains limited.

The growth accident model, in which grain boundary migration velocity and grain boundary migration distance are expected to be the two promoting factors of annealing twin formation, is most commonly used for explaining twin formation [5–8]. In this model, annealing twin formation is related to grain boundary migration. However, the exact relationship between these two phenomena is not clear. Gleiter and Pande [5, 6] derived models based on growth accidents to predict twin density evolution. In Gleiter's model, the twin formation probability is mainly determined by grain boundary mobility and migration driving force [5] and makes no distinction as to the type of driving force. Accordingly, the annealing temperature influences the twin formation probability through its effect on grain boundary mobility. In Pande's model, however, the number of twin boundaries per grain is proportional to the variation in grain size and grain boundary migration driving force, and is not sensitive to the annealing temperature [6]. Subsequently, other works addressed the impact of processing and microstructural factors on annealing twin formation. Studies aimed to maximize annealing twin boundary content mainly by varying prior cold deformation level and annealing temperature and were conducted on commercially pure nickel [9–11]. The low deformation strains (<10 %) meant that these studies were limited to the case of strain-induced grain boundary migration (SIBM). In our previous work [12], through an in situ experiment, we confirmed that annealing twins are mainly formed during recrystallization [13]. Some recent studies were performed to analyze twin formation in the recrystallization regime. Li et al. [14] studied the role of deformation temperature and strain while performing grain boundary engineering in Inconel 600. Nevertheless, due to the complexity of

✉ Y. Jin  
yuan.jin@mines-paristech.fr

<sup>1</sup> MINES ParisTech, PSL - Research University, CEMEF - Centre de mise en forme des matériaux, CNRS UMR 7635, CS 10207 rue Claude Daunesse, 06904 Sophia Antipolis Cedex, France

<sup>2</sup> Carnegie Mellon University, 5000 Forbes Avenue, Pittsburgh 15213, USA

microstructural evolution during hot deformation, the precise roles of these parameters on annealing twin development could not be determined. Wang et al. [15] analyzed the influence of stored energy on twin formation during primary recrystallization in a nickel-based alloy and concluded that the number of twin boundaries per grain increases with increasing stored energy level. However, in this study, annealing twins were quantified only at the end of recrystallization and only the number of twins per grain was considered. In addition, Bair et al. [16] found that the heating velocity could also promote annealing twin content during recrystallization of pure nickel. However, the actual values of the applied heating rates were not given in that study. Recently, the effect of annealing temperature on annealing twin evolution during recrystallization was addressed in [17] for cold-rolled pure nickel and [18] for a nickel-based alloy. In both works, samples underwent heat treatments at different temperatures for a fixed duration. Depending on temperature, the obtained microstructures corresponded to different stages of recrystallization and grain growth. Therefore, these two studies do not allow a precise analysis of the annealing twin content at the end of recrystallization. Furthermore, the role of prior deformation level on annealing twin content was also investigated in [18], but only within the grain growth regime.

The present paper aims at establishing the influence of three thermo-mechanical factors (i.e., stored energy level, annealing temperature, and heating velocity) and one microstructural factor (i.e., initial grain size) on annealing twin formation during static recrystallization of commercially pure nickel. Since annealing twin content can be interpreted differently via different quantification methods [11, 19, 20], three different annealing twin quantification methods, viz. twin density, number of twin boundaries per grain and twin boundary length fraction, are used. The experiments and results related to the influence of temperature and strain on the one hand and of heating rate and initial grain size on the other hand are presented in the third and fourth sections, respectively. A new proposition for how the recrystallization front morphology affects the annealing twin formation is presented in the fifth section, as a consistent explanation of the whole set of results.

## Experimental and data processing details

Commercially pure nickel (99.999 wt% obtained from Alfa Aesar) was used in the present study. Two distinct series of experiments were performed to analyze the influences a) of prior deformation amount versus annealing temperature and b) of heating velocity on annealing twin formation during recrystallization. A different initial grain size was

used in the “heating rate experiments” to assess the influence of that microstructural parameter.

All samples (initially fully recrystallized) were submitted to compression tests at room temperature and subsequently annealed at a temperature between 350 and 550 °C.

Microstructures were quantitatively analyzed by Electron BackScatter Diffraction (EBSD). Specific experimental details are given in “[Experimental details](#)” sections.

The OIM<sup>TM</sup> software was used to analyze the EBSD data. The recrystallized grains were defined in the EBSD maps using the criterion that the grain orientation spread (GOS) was less than 1° [21]. GOS is defined as the average of the misorientation angles between the orientation of each point inside a grain and the average orientation of that grain. For grain detection, the minimum misorientation angle to define a high-angle grain boundary was set to 15°. Annealing twins are defined by a misorientation of 60° about the <111> axis with a tolerance of 8.66°, according to Brandon’s criterion [22], regardless of their coherent versus incoherent character.

Three different quantities were used to quantify annealing twins: the annealing twin density ( $N_L$ ), the number of annealing twin boundaries per grain ( $N_G$ ), and the twin boundary length fraction ( $L\%$ ), respectively, which are defined as

$$N_L = \frac{L_{tb}}{S} \times \frac{2}{\pi}, \quad (1)$$

$$N_G = \frac{N_2 - N_1}{N_1}, \quad (2)$$

$$L\% = \frac{L_{tb}}{L_{HAB}} \times 100, \quad (3)$$

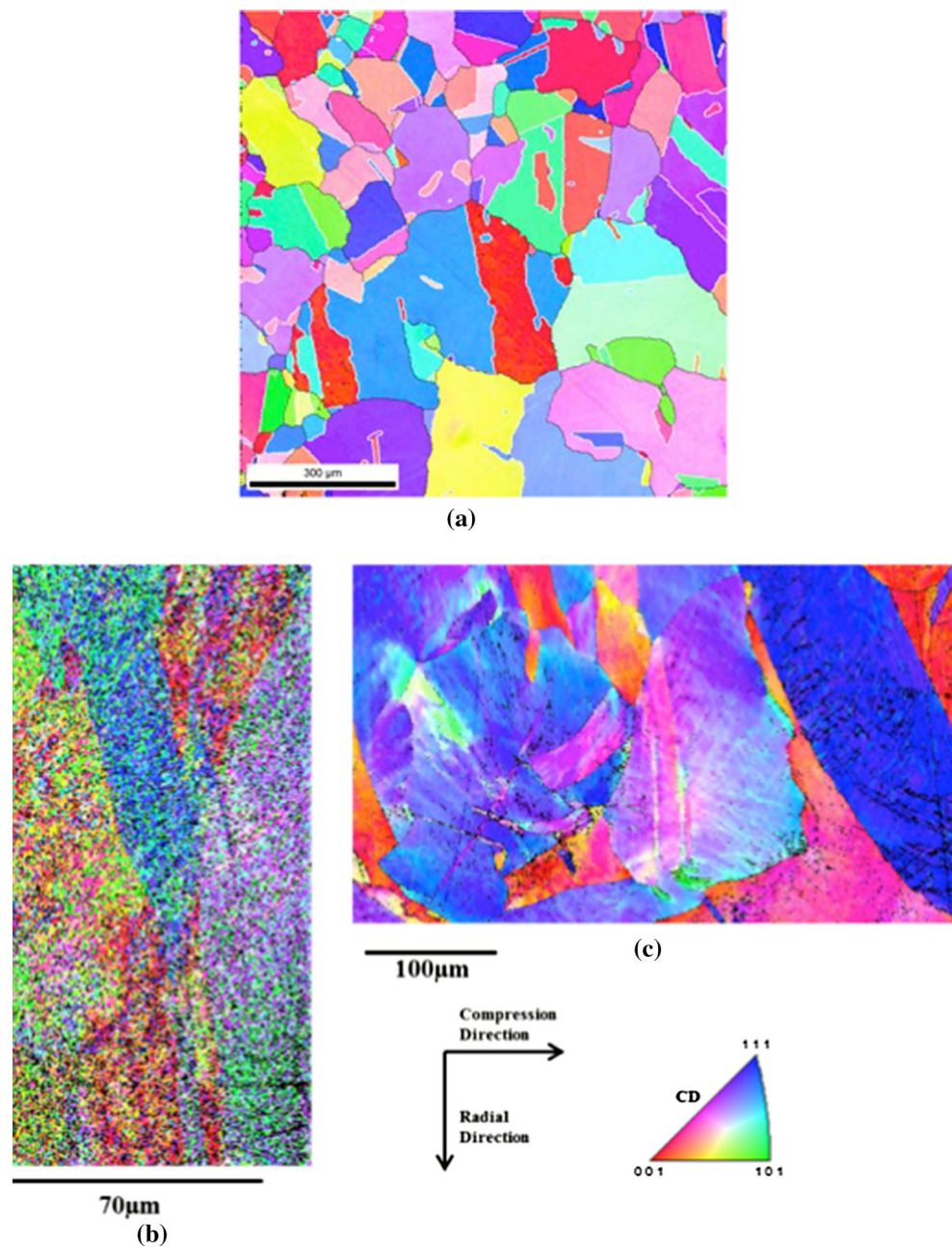
where  $L_{tb}$  is the twin boundary length detected in a given sample section area  $S$ ,  $N_1$  is the number of grains ignoring  $\Sigma 3$  boundaries in the grain detection procedure,  $N_2$  is the number of grains by considering  $\Sigma 3$  boundaries as grain boundaries, and  $L_{HAB}$  is the length of all the high-angle grain boundaries including  $\Sigma 3$ .

## Influence of prior deformation level and annealing temperature

### Experimental details

Two cylindrical samples, 5 mm in diameter and 8 mm in height with a fully recrystallized microstructure (average GOS of 0.6°, which is close to the angular resolution of EBSD under the acquisition settings that were used) and an average grain size (arithmetic mean) of 90  $\mu\text{m}$ , Fig. 1a,

**Fig. 1** EBSD map of the state of the material before (a) and after 60 % (b) and 30 % (c) height reduction by compression at room temperature; the microstructure is shown within an orientation color-coded scale (Compression Direction CD) projected in the standard *triangle*; Unreliable pixels are plotted *black* and will not be further considered



were compressed at room temperature to 30 or 60 % height reduction. The corresponding macroscopic true strains ( $\varepsilon$ ) are indicated in Table 1. The compressed samples were then cut into semi-cylinders, which were then annealed at 350 or 450 °C to perform recrystallization. Several annealing steps were performed on the same samples until recrystallization was complete. The microstructure  $X_{RY}$  refers to the sample with  $X$  % deformation level and recrystallized at  $Y$  °C. The heating device was a Thermo Scientific™ Lindberg/Blue M™ MiniMite™ tube furnace. EBSD characterizations were performed in an FEI

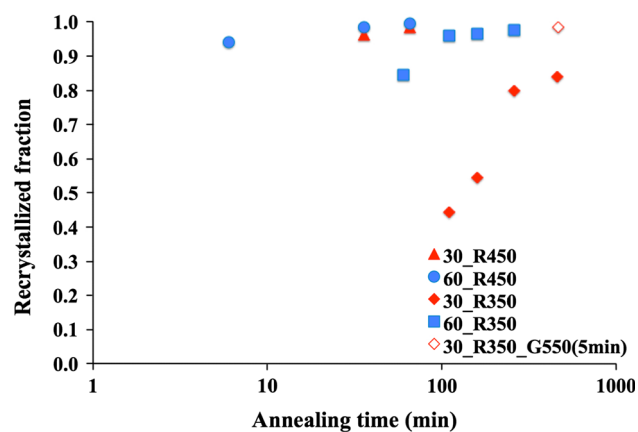
XL30 ESEM microscope equipped with a TSL EBSD system. EBSD orientation maps, which all have the same size (800  $\mu\text{m}$   $\times$  800  $\mu\text{m}$ ), were recorded with a 1.2- $\mu\text{m}$  step size. At the end of recrystallization, the EBSD maps contained 100–500 recrystallized grains depending on the thermo-mechanical history (twin boundaries being ignored and grains with equivalent diameter smaller than 3  $\mu\text{m}$  not considered). It is worth mentioning that the average grain size calculated based on the EBSD maps with a low grain count (e.g., 100) may diverge appreciably from the true value.

**Table 1** Annealing twin quantification and grain size in the four samples after the completion of recrystallization

	350 °C	450 °C
30 %	<b>30_R350</b>	<b>30_R450</b>
	$\varepsilon = 0.36$	$\varepsilon = 0.36$
	$\bar{D} = 60 \mu\text{m}$	$\bar{D} = 65 \mu\text{m}$
	$N_L = 29 \text{mm}^{-1}$	$N_L = 31 \text{mm}^{-1}$
	$N_G = 10.6$	$N_G = 10.5$
	$f_L = 0.64$	$f_L = 0.66$
60 %	<b>60_R350</b>	<b>60_R450</b>
	$\varepsilon = 0.91$	$\varepsilon = 0.91$
	$\bar{D} = 34 \mu\text{m}$	$\bar{D} = 32 \mu\text{m}$
	$N_L = 46.4 \text{mm}^{-1}$	$N_L = 44.8 \text{mm}^{-1}$
	$N_G = 6.7$	$N_G = 6$
	$f_L = 0.55$	$f_L = 0.53$

### Experimental results

The EBSD maps in Fig. 1 illustrate the microstructure in the initial state and after 60 and 30 % height reduction, observed in the longitudinal cross-section. The two deformation levels can be qualitatively distinguished by the gradient of the IPF colors. However, the resolution of the EBSD map does not allow for capturing the fine details of the microstructure of the 60 % deformed sample. The overall recrystallization kinetics is illustrated in Fig. 2. Owing to the rapidity of recrystallization, the early recrystallization stages were not captured in the samples annealed at 450 °C (60\_R450 and 30\_R450). On the other hand at 350 °C, for 60\_R350, it took as long as 260 min to complete recrystallization and for 30\_R350, recrystallization was still not completed after 460 min. For the latter, the annealing temperature was subsequently increased to 550 °C for an additional 5-min annealing to achieve full recrystallization.

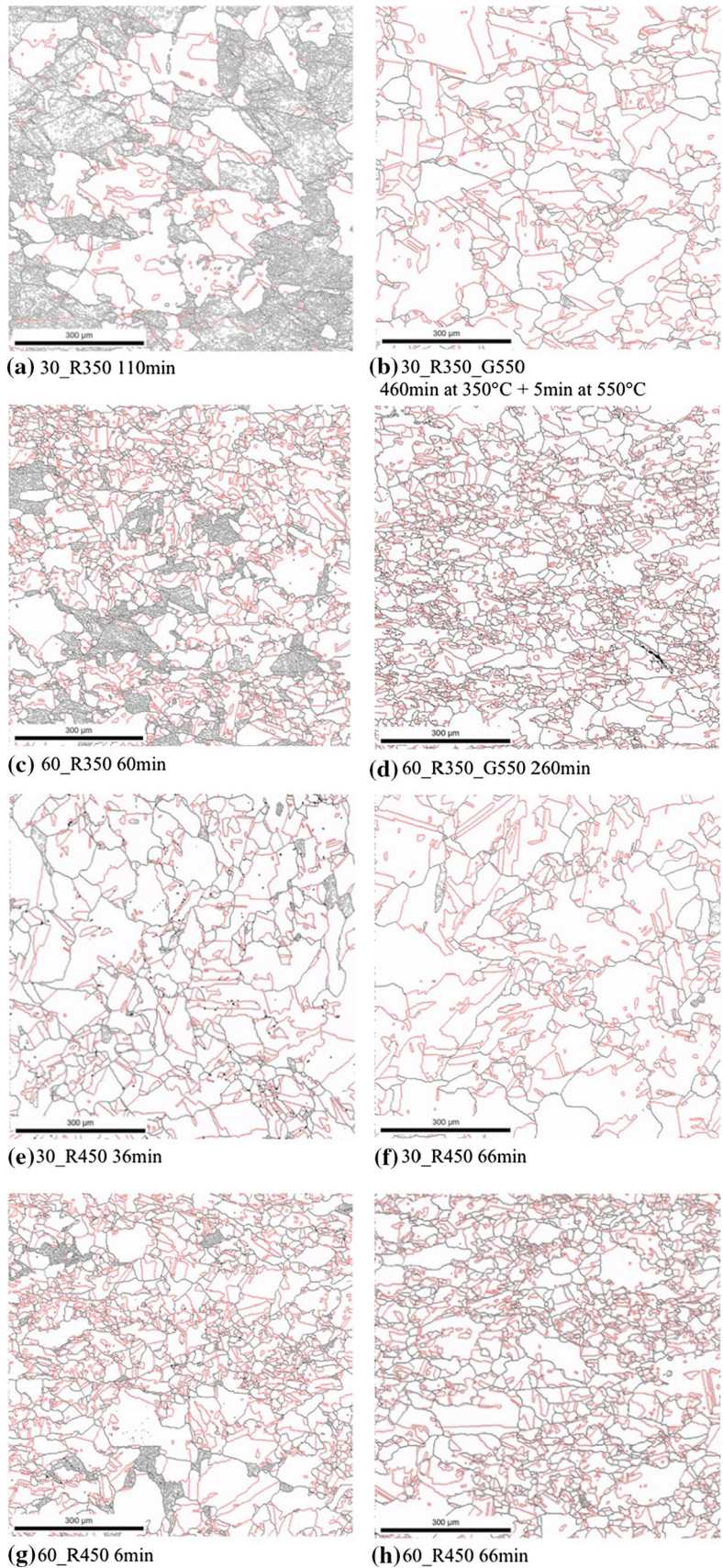
**Fig. 2** Recrystallization kinetics at 350 or 450 °C after 30 or 60 % height reduction by compression at room temperature

The microstructural evolution in the four samples during recrystallization is illustrated in Fig. 3. Despite the difference in recrystallization kinetics, the samples with the same deformation level but annealed at different temperatures (e.g., 60\_R450 and 60\_R350) have similar microstructures. The twin density evolutions in the four samples are plotted as a function of the recrystallization fraction in Fig. 4a and as a function of the average recrystallized grain size in Fig. 4b. With a greater amount of stored energy, the twin density at the end of recrystallization is higher. This observation is consistent with experimental results reported previously in nickel-based superalloys [15, 23]. Meanwhile, the annealing temperature, in the present range, has no obvious effect on annealing twin development during recrystallization, which is consistent with another experimental result reported recently in nickel [16], but contrary to the Gleiter's model, in which annealing temperature should influence the twin formation probability [5].

The arithmetic average grain size ( $\bar{D}$ ) and the annealing twin content at the end of the recrystallization regime were primarily determined by the deformation level but not the annealing temperature, as indicated in Table 1 and visible on Fig. 4. Meanwhile, the number of twin boundaries per grain and the twin boundary length fraction (given in Table 1) exhibit an inverse trend from the twin density in those annealing twin quantifications. As indicated by Eq. 1, the twin density is solely determined by the twin boundary length after the completion of recrystallization. On the other hand, the twin boundary length fraction, Eq. 3, is inversely proportional to the total grain boundary length. Higher deformation levels result in smaller final recrystallized grain size [24]. Smaller recrystallized grain size results in greater total grain boundary length (per unit area). Therefore, in contrast to the twin density, the annealing twin length fraction decreases with higher deformation levels.

In the growth accident model, the grain boundary migration distance and the grain boundary migration driving force are considered as two key factors promoting the generation of annealing twins. During recrystallization, the driving force for recrystallization front migration is dominated by the stored energy level, which increases with the prior cold deformation. Consistently, greater deformation resulted in more twin boundaries per unit length, thus to higher twin density in the overall microstructure. Meanwhile, the number of twin boundaries per grain, Eq. 2, depends also on the grain boundary migration distance, which can be considered here to be half of the recrystallized grain diameter. In the samples with different average final recrystallized grain sizes, due to the difference in grain boundary migration distance, the average number of twin boundaries per grain cannot solely reflect the effect of grain boundary migration driving force.

**Fig. 3** Microstructure evolution during recrystallization at 350 and 450 °C after cold compression to 30 or 60 %; low-angle grain boundaries ( $1^{\circ}$ – $15^{\circ}$ ) are shown as *gray thin lines* with high angle boundaries shown as *black lines*; twin boundaries within Brandon’s tolerance criterion are plotted *red*; the sample reference and the corresponding cumulative annealing time are indicated under each map (Color figure online)



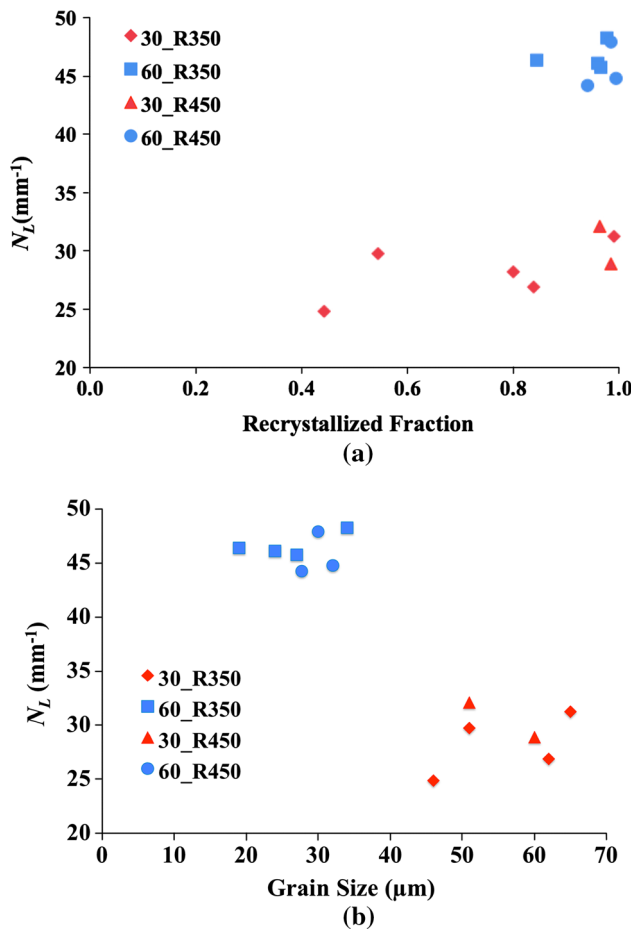


**Fig. 4** Annealing twin density evolution during recrystallization, plotted as a function of (a) recrystallization fraction (b) average recrystallized grain size, at 350 or 450 °C after 30 or 60 % height reduction by compression at room temperature

For the purpose of eliminating the effect of recrystallized grain size on annealing twin content interpretation, three grains having similar sizes (equivalent circle grain diameter of about 140  $\mu\text{m}$ ) were selected in each of the four samples at the end of recrystallization (colored in Fig. 5), and twin contents inside these grains were compared. Relatively large grains were selected, as small grains in the observed 2D section can be large ones in 3D. Those three grains account for 27–33 % of the surface area of the EBSD maps in each state. In addition, the grains were selected in such a way that they were not in contact with the borders of the EBSD acquisition area to correctly calculate the number of twin boundaries per grain and the equivalent grain size. The number of twin boundaries per grain and twin density confirm the conclusions drawn from the overall average values (Table 2): higher stored energy level promotes annealing twin formation during recrystallization and the effect of annealing temperature on annealing twin formation is negligible within the investigated range.

In addition, we re-emphasize that different final recrystallized grain sizes may lead to different interpretations of the twin content in the overall microstructure depending on the quantification methods used.

## Discussion

As expected, the recrystallization kinetics were accelerated by higher prior cold deformation amount and higher annealing temperature. During recrystallization, the driving force for recrystallization front migration depends mainly on the stored energy level, which increases with the cold deformation amount. Besides, the grain boundary mobility generally increases with temperature [25]. Thus, the recrystallization front migration velocity increases with both the deformation amount and the annealing temperature through their effects on driving force and mobility, respectively. An issue still requiring clarification is why annealing twin formation is promoted by the grain boundary migration velocity. From an atomistic point of view, two types of atomic motions can be depicted during grain boundary migration in molecular dynamic simulations [26, 27]:

Type 1: string-like cooperative motions parallel to the grain boundary plane;

Type 2: single-atom jumps across the grain boundary plane.

Type 2 controls the rate of boundary migration and is necessary to redistribute the free volume to allow for Type 1 motion [26]. With higher driving force and higher annealing temperature, the characteristic times associated with both types decrease [26, 28]. These two types of motions, that cause the atoms to change from one grain orientation to another, are very likely to be related to the formation of annealing twins, especially Type 1 which controls the position of the latest added atoms on the underlying atomic plane. However, the exact role of atomic movement inside grain boundaries on annealing twin formation is not clear, especially due to the complex structure of high angle boundaries [28]. The explanation of annealing twin formation at an atomistic scale requires thus a more detailed and targeted study.

## Influence of heating velocity

### Experimental details

A cylindrical sample, 5 mm in diameter and 8 mm in height, was used. The initial microstructure, fully recrystallized (average GOS equal to 0.6°) with an average grain size (arithmetic mean) equal to 16  $\mu\text{m}$ , is described in Fig. 6a. The sample was then compressed at room

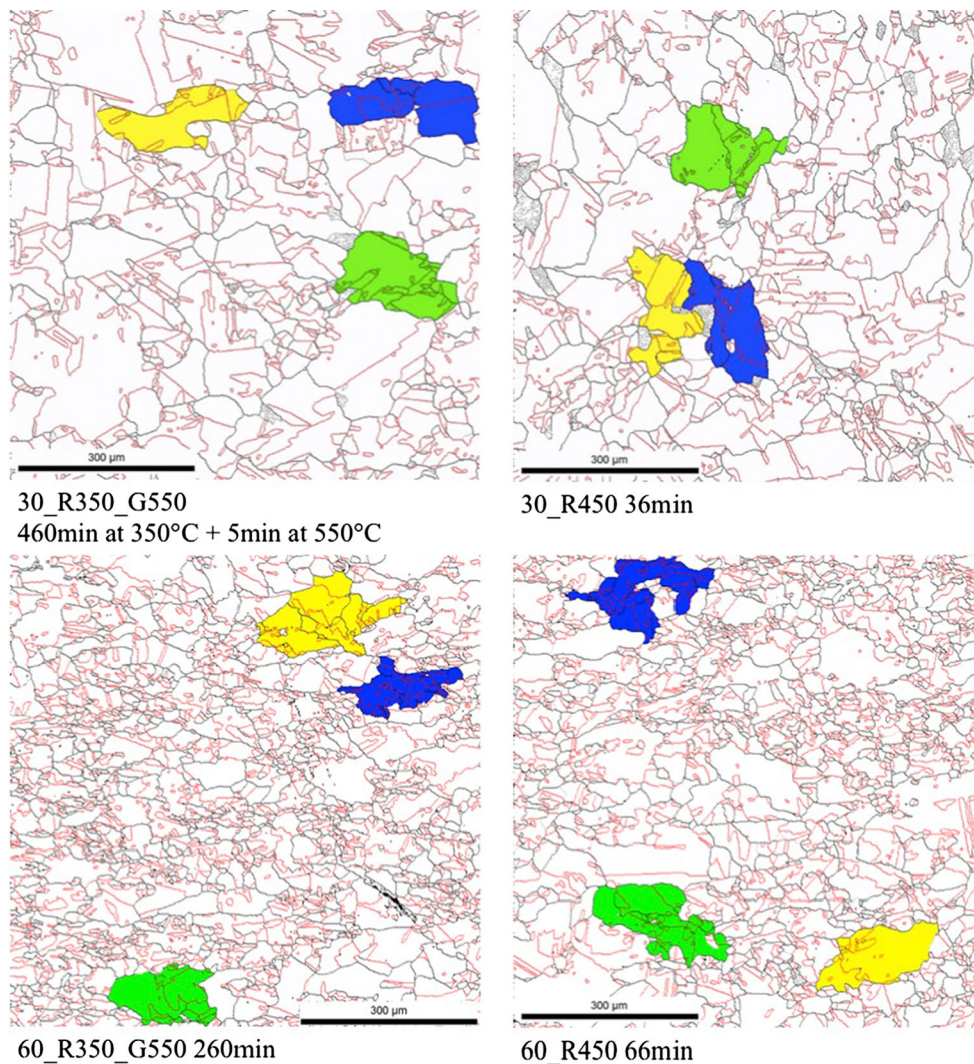


**Fig. 5** Selected recrystallized grains having similar grain sizes in the four samples at the end of recrystallization; the annealing temperature and the corresponding cumulative annealing time are indicated under each map (Color figure online)

**Table 2** Average annealing twin contents obtained, thanks to different twin quantification methods and grain size of the three selected grains after recrystallization completion

	350 °C	450 °C
30 %	<b>30_R350</b> $\bar{D} = 150 \mu\text{m}$ $N_L = 29 \text{ mm}^{-1}$ $N_G = 22$	<b>30_R450</b> $\bar{D} = 143 \mu\text{m}$ $N_L = 28.5 \text{ mm}^{-1}$ $N_G = 19$
60 %	<b>60_R350</b> $\bar{D} = 135 \mu\text{m}$ $N_L = 46 \text{ mm}^{-1}$ $N_G = 42$	<b>60_R450</b> $\bar{D} = 141 \mu\text{m}$ $N_L = 41 \text{ mm}^{-1}$ $N_G = 38$

temperature to 50 % height reduction, and the resulting microstructure is shown in Fig. 6b. The compressed sample was cut into two semi-cylinders. These two samples

referred to as V500 and V5 were then heated to 350 °C at 500 and 5 °C/min, respectively, to recrystallize them. Several annealing steps were performed on the same samples until recrystallization was complete. The cooling rate was identical for the two samples, ~200 °C/min. The EBSD characterizations were performed in a ZEISS SUPRA 40 FEG SEM equipped with a Bruker CrystAlign EBSD system. The step size for EBSD map acquisition was 0.46 μm. Grains were detected with a threshold angle at 15°, twin boundaries being ignored. The grains with an equivalent circle diameter smaller than 1 μm were not considered in this analysis.

**Experimental results**

The microstructural evolution in both samples during recrystallization is illustrated in Fig. 7. In each sample, an

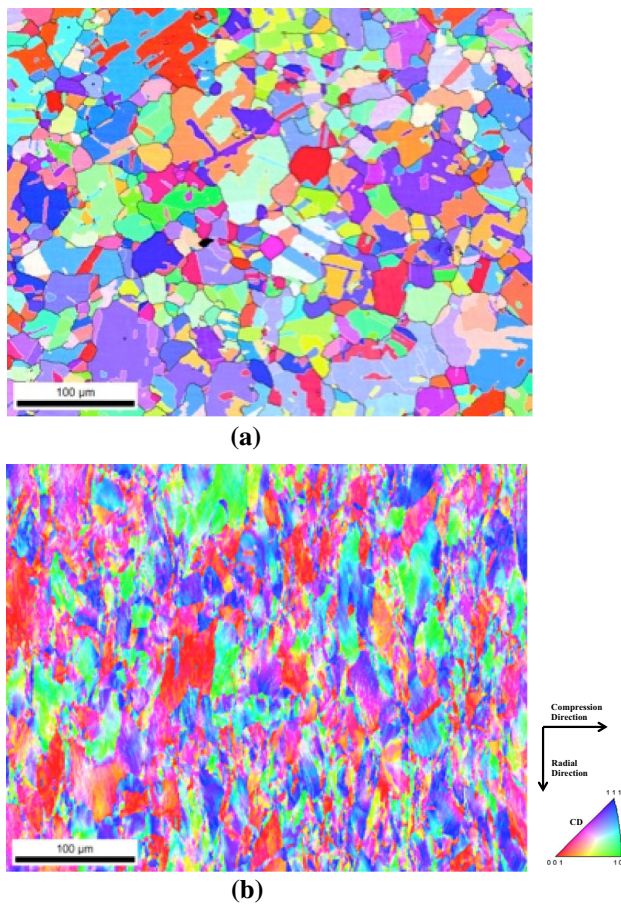


**Fig. 6** EBSD map of the state of the material before (a) and after (b) 50 % height reduction by compression at room temperature

almost fully recrystallized microstructure (about 94 %) was obtained at the end of the heat treatment series. The cumulative annealing time at 350 °C is much shorter for V5 than for V500. This phenomenon is consistent with another study recently published by Bair et al. [16]. As indicated in Fig. 7, about 70 % of the microstructure was recrystallized in V5 at the moment when the annealing temperature was reached. Meanwhile, in V500, the recrystallization fraction was only 22 % after a 1-min annealing at 350 °C. Therefore, different from the almost instantaneous heat up in V500, recrystallization initiated during heating in V5, which decreased the annealing time to complete recrystallization at 350 °C.

The twin densities in both samples are expressed as a function of the recrystallization fraction, Fig. 8a, and as a function of the average recrystallized grain size, Fig. 8b. Despite the difference in recrystallization kinetics, for the same recrystallization fraction, the twin densities in the two samples are almost identical. In addition to the twin density, the length fraction of annealing twin boundaries and the number of twin boundaries per grain in the overall microstructure at the end of the recrystallization regime were calculated for both samples, Table 3.

At near-complete recrystallization, the average grain sizes (arithmetic mean) and the twin contents including  $N_L$ ,  $N_G$ , and  $f_L$  are very close in V5 and V500. This observation indicates that the heating velocity, within the present range, influences neither the grain size nor the twin content during the course of recrystallization.

## Discussion

Our results indicate that the heating rate has a negligible effect on annealing twin development during recrystallization. However, in the work reported recently by Bair et al. [16] about twin formation during recrystallization, also in nickel, the twin boundary fraction ( $f_L$ ) increased with decreasing heating rate. In the latter work, the thermo-mechanical path has some differences with the one we designed for our experiments, e.g., the annealing temperature is higher (600–750 °C). In addition, the difference in the applied heating rates is not given. Details are missing in the paper, which makes it difficult to make a direct comparison to the current work.

In this section, the height reduction of the sample was 50 %. However, the twin density at the end of the recrystallization regime is much higher as compared to the samples with 60 % height reduction in the series of “Influence of prior deformation level and annealing temperature” section. The initial grain size before deformation was 90 μm in the 60 % compressed sample, Fig. 1a, but only 16 μm for the 50 % compressed samples Fig. 6a. This difference is likely to be responsible for the difference in twin density. A fine-grained initial microstructure leads to a more random distribution of recrystallization nucleation sites [29]. Randomly distributed recrystallization nuclei can grow independently at the early stage of recrystallization before impingement with other nuclei. In a previous study [12], annealing twins are reported to be formed mostly before the impingement of recrystallized grains, since the impingement decelerates the growth of individual recrystallized grains. Therefore, as illustrated in Fig. 8, after a 1-min annealing (about 20 % recrystallized), the twin density in the recrystallized part of sample V500 (higher than 80 mm<sup>-1</sup>) is much higher than in the initially coarse-grained samples. Since the annealing twin formation decelerated after the impingement of recrystallized grains in both initially fine-grained and coarse-grained samples, this difference created at the beginning of recrystallization could result in a difference in annealing twin density at the end of recrystallization.

## On the influence of the recrystallization front tortuosity

In the experiment aimed at testing the impact of prior deformation level and annealing temperature, only the deformation level but not the annealing temperature



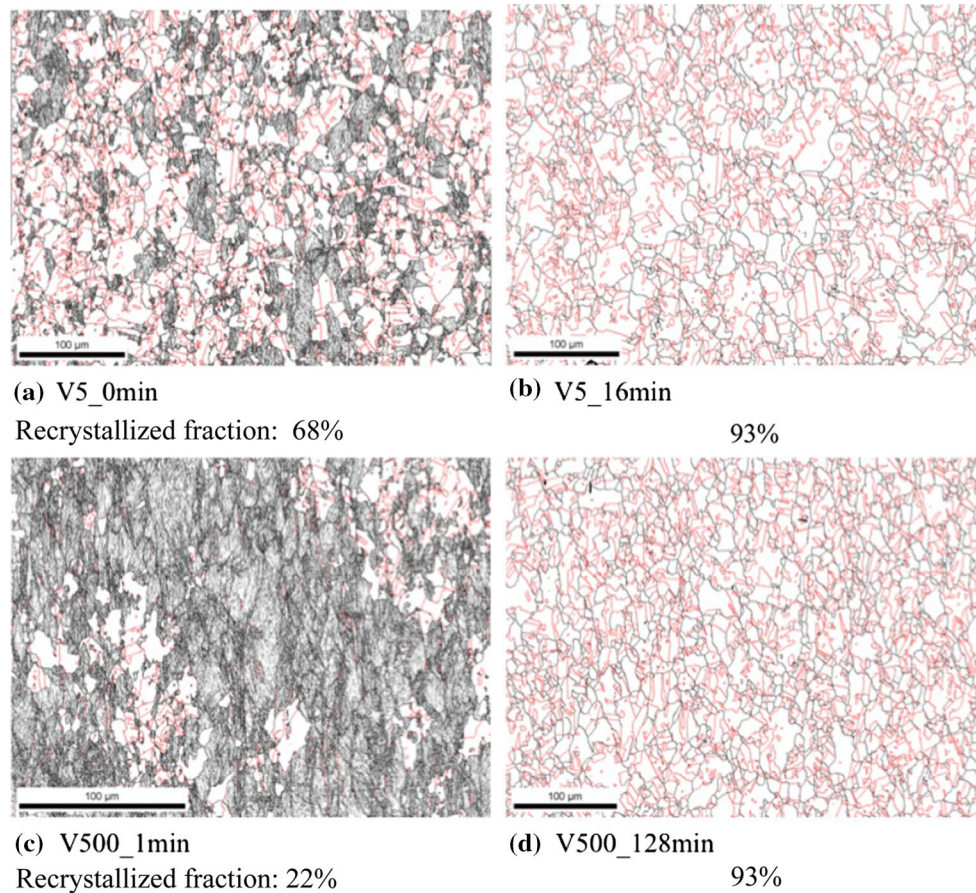


**Fig. 7** Microstructure evolution during annealing at 350 °C after heating at either 5 °C/min (samples labeled V5\_Xmin) or 500 °C/min (V500\_Xmin); the annealing time and the corresponding recrystallization fraction are given below each map. The microstructure V5\_0 min (a) was obtained by heating the sample up to 350 °C at

5 °C/min and cooling down immediately. Low-angle grain boundaries (1°–15°) are shown as *gray thin lines* with high angle boundaries shown as *black thick lines*; the *red lines* denote  $\Sigma 3$  boundaries (Color figure online)

promoted the annealing twin formation within the present range. This result suggests that the grain boundary migration velocity influences annealing twin formation only through the effect of the migration driving force, which appears to be consistent with Pande's model [6].

The numbers of annealing twin boundaries per grain,  $N_G$ , in the six analyzed samples in the present study [12] are plotted as a function of the average grain size in Fig. 9. The average  $N_G$  in the overall recrystallized microstructure increased continuously during recrystallization. Meanwhile, the correlation between  $N_G$  and the average grain size depends on the whole thermo-mechanical history of the sample, e.g., the deformation amount and the initial grain size before deformation. (Not shown here:  $N_G$  was also calculated in the five largest grains in each microstructure. The evolution of  $N_G$  in the largest grains is very similar to that of the average value in the overall recrystallized microstructure.) As mentioned, in Pande's model, the grain boundary migration driving force and the

grain boundary migration distance are supposed to be the only two factors influencing annealing twin formation. However, in the present study, the initial grain size before deformation, which could not influence significantly the average recrystallization front migration driving force, influences considerably the annealing twin development during recrystallization. Therefore, we need a new approach to explain annealing twin formation mechanisms and their dependence on thermo-mechanical history.

In the previous paper [12], we proposed a semi-atomistic model to explain the relationship between annealing twin formation and grain boundary curvature. According to this model, annealing twins are more likely to be formed behind the convex portions of the recrystallization front. In practice, annealing twins are mostly generated during recrystallization and behind the migrating recrystallization front(s). Following the growth accident model, a twin is more likely to form if the recrystallization front, or at least a portion of it, has {111} facets. Those facets are wider if

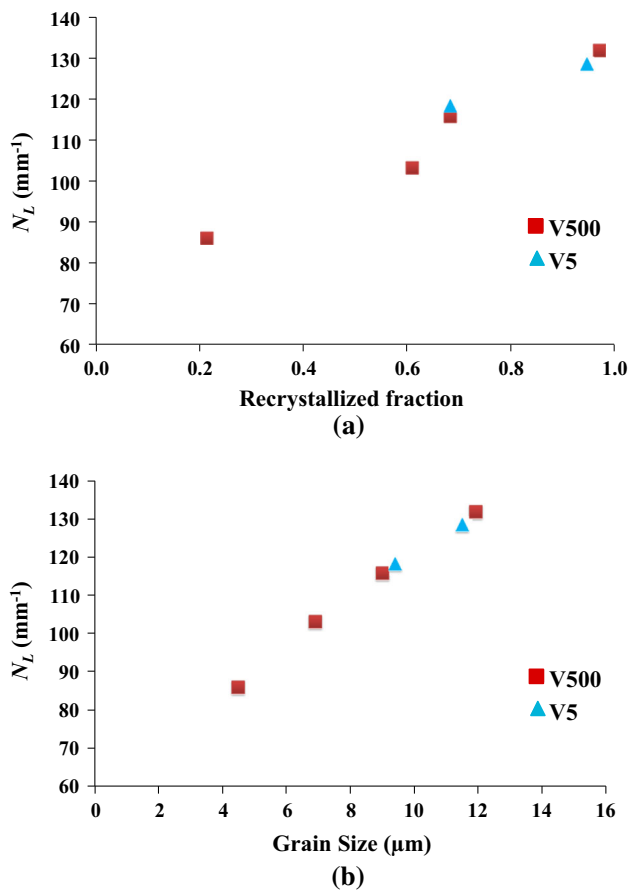


**Fig. 8** Annealing twin density evolution in the two samples during recrystallization (at 350 °C) plotted as a function of (a) recrystallization fraction and (b) recrystallized grain size

**Table 3** Annealing twin measurements and grain size for the two different heating rates after the completion of recrystallization

Ref	$\bar{D}$ ( $\mu\text{m}$ )	$N_L$ ( $\text{mm}^{-1}$ )	$f_L$	$N_G$
V5	11	128.5	0.56	3.1
V500	11.5	131	0.55	3.4

the front is close to being parallel to  $\{111\}$  (at the mesoscopic scale). As schematized in Fig. 10a, the more tortuous the recrystallization front is, the higher is the probability to find portions of it parallel to any given kind of plane but especially to  $\{111\}$  (arrowed on Fig. 10a). Among those  $\{111\}$  portions, those moving opposite to their curvature (double arrows) are more likely to form coherent twins according to the principle described in the previous study [12].

For a rough recrystallization front, the variations in local curvature should therefore lead to more potential sites for annealing twin generation. Overall, this implies that the recrystallization front tortuosity could also influence

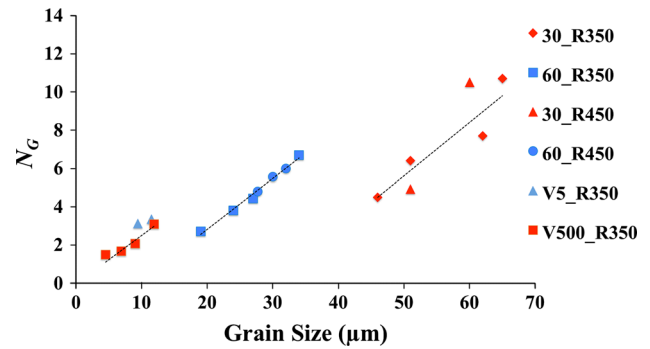


**Fig. 9** The average number of annealing twin boundaries per grain in the overall recrystallized microstructure plotted as a function of the average recrystallized grain size in the six analyzed samples

annealing twin formation during recrystallization. Therefore, we quantified the recrystallization front tortuosity within our EBSD maps (i.e., at the mesoscopic scale).

According to Epstein [30], the tortuosity of the recrystallization front ( $\tau$ ) can be calculated by a simple relationship:

$$\tau = \frac{L_{\text{RF}}}{R}, \quad (4)$$

where  $L_{\text{RF}}$  is the length of the recrystallization front (geodesic length) and  $R$  is the end-to-end length of the recrystallization front (Euclidean length). With Eq. 4, and as illustrated in Fig. 10, the average tortuosity of the recrystallization front in the overall microstructure was calculated with the following steps within the OIM software:

1. Reconstruct the high-angle grain boundaries (twin boundaries excluded) in the overall microstructure based on the triple junctions (blue segments in Fig. 11a). The maximum deviation between reconstructed boundary and corresponding boundary segments is 30 times the EBSD acquisition step sizes (e.g., 36  $\mu\text{m}$  for the EBSD maps shown in Fig. 3). It is worth mentioning that the applied deviation (30 pixels) is the maximum value allowed in the OIM software. For the considered EBSD maps, with this value, nearly all of the high-angle grain boundaries defined between two triple junctions can be reconstructed by a single straight line.
2. Calculate the total length of high-angle grain boundaries in the overall microstructure ( $L_{\text{GB}}^0$ ) (twin boundaries are excluded) and the total length of the corresponding reconstructed boundaries ( $R^0$ ).
3. Repeat step 1 and step 2 inside the deformed matrix only and the recrystallized part only as indicated, respectively, in Fig. 11b and c.  $L_{\text{GB}}^{\text{Rex}}$ ,  $L_{\text{GB}}^{\text{Def}}$ ,  $R^{\text{Rex}}$ , and  $R^{\text{Def}}$  denote, respectively, the length of high-angle grain boundaries inside all the recrystallized grains and the deformed matrix, and the length of reconstructed boundaries inside all the recrystallized grains and the

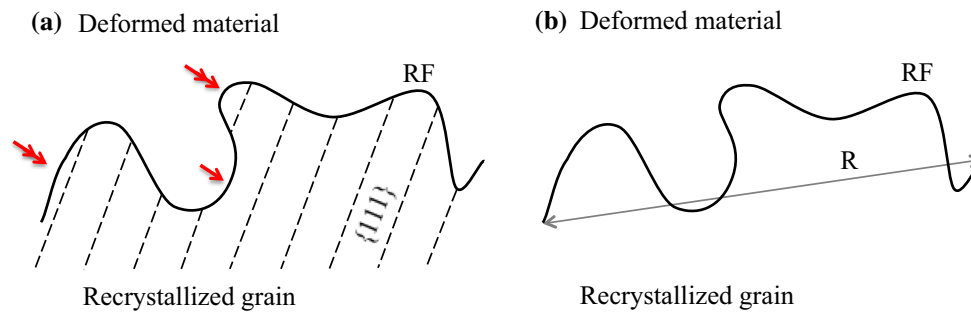
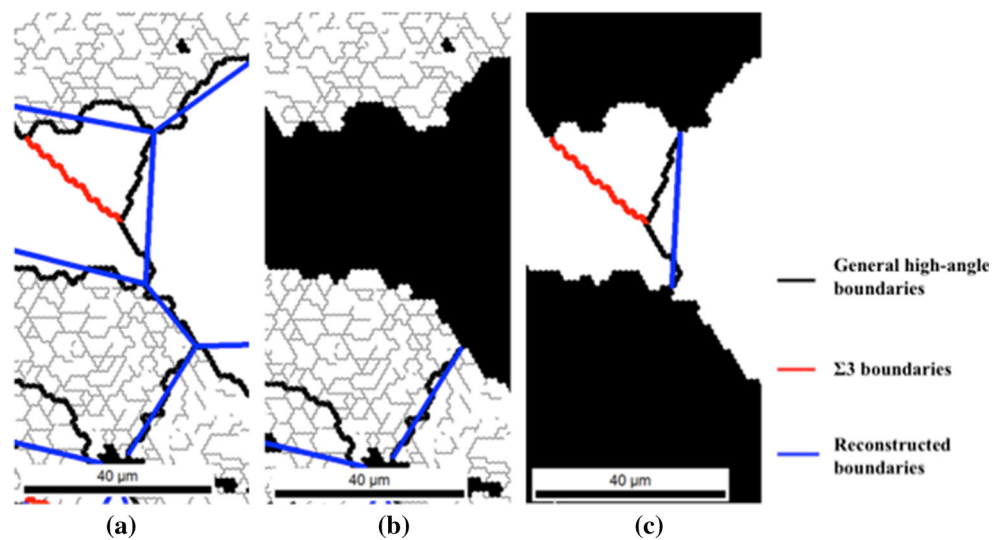


**Fig. 10** **a** Schematic of a recrystallization front (RF) with portions close to be parallel to {111} (*arrowed*). Following the principle proposed on Fig. 2.26, the convex ones, moving opposite to their curvature (*double arrows*), are potential sites for perfect coherent twins; the concave ones moving towards their curvature center

(*simple arrow*) can only lead to coherent segments associated with incoherent ones which may further migrate and make the new twin annihilate. **b** Same recrystallization front (RF) and its end-to-end length (R)

**Fig. 11** Schematic of recrystallization front tortuosity calculation procedure; **a** the overall microstructure; **b** the non-recrystallized part; **c** the recrystallized part. Low-angle grain boundaries ( $1^{\circ}$ – $15^{\circ}$ ) are shown as *gray thin lines*, *black lines* are the general boundaries with a disorientation higher than  $15^{\circ}$ , *red lines* are  $\Sigma 3$  boundaries (within the Brandon’s criterion), and *blue lines* are the reconstructed grain boundary segments (with a parameter for the allowed distance to the boundary of 30 pixels) (Color figure online)



deformed matrix. Those values do not include the recrystallization front lengths.

- The lengths of the recrystallization front and of the corresponding reconstructed boundaries are then calculated using the following:

$$L_{RF} = L_{GB}^0 - (L_{GB}^{Rex} + L_{GB}^{Def}), \tag{5}$$

$$R = R^0 - (R^{Rex} + R^{Def}). \tag{6}$$

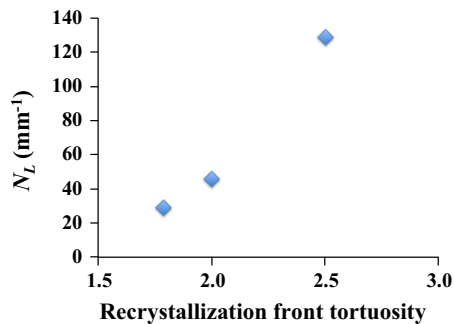
The tortuosity of the recrystallization front was calculated in the three EBSD maps 30\_350\_110, 60\_350\_60, and V5\_0 min where the recrystallization is in progress and recrystallized grains impinge on each other, forming clusters. As the deviation between reconstructed boundary and the corresponding boundary segments is defined by the EBSD acquisition step size, for the sake of consistency, the step size of the EBSD map of V5\_0 min was converted from  $0.46 \mu\text{m}$  to  $1.38 \mu\text{m}$ , which is close to the step size used the experiment aiming at testing the impact of prior

deformation level and annealing temperature ( $1.2 \mu\text{m}$ ), before applying the above procedure. As indicated in Table 4 and in Fig. 12, the recrystallization front tortuosity during recrystallization is positively correlated with the annealing twin density at the end of recrystallization.

This observation is consistent with our idea that the variation in local curvature of the recrystallization front could promote annealing twin formation by providing more potential nucleation sites. The tortuosity of a migrating recrystallization front is found to arise when the stored energy level in the adjacent deformed matrix is non-uniform [31]. Indeed the stored energy level determines the driving force for recrystallization migration. Thus, the local fluctuation in stored energy level introduces local variation in recrystallization front migration velocity, which changes the local morphology of the front. This local migration and its relation to annealing twin formation were previously reported in Inconel 600 [32]. This rationale may also explain the effect of deformation amount and the initial grain size before deformation on annealing twin formation

**Table 4** Recrystallization front tortuosity calculated in samples 30\_R350, 60\_R350, and V5

Ref	$L_{RF}$ (mm)	$R$ (mm)	$\tau$	Rex fraction	$N_L$ ( $\text{mm}^{-1}$ ) at the end of Rex
30_R350_110 min	13.1	7.9	1.79	0.46	29
60_R350_60 min	15.2	7.6	2	0.84	46
V5_0 min	17.3	6.9	2.5	0.61	128.5

**Fig. 12** Annealing twin density at the end of recrystallization as a function of recrystallization front tortuosity, showing a positive correlation between the two quantities

observed in the present study through their influence on the fluctuations in the stored energy field. It is unclear whether increasing strain tends to homogenize or on the contrary to make the strain field more heterogeneous, considerations which are in addition very much scale dependent. There could be different answers depending on the strain range, on the material plasticity anisotropy, on its crystallographic texture, and many other microstructure properties. A dedicated study must be performed to answer such questions. On the other hand, prior grain boundaries give rise for sure to locally large orientation gradient due to strain incompatibility between the neighboring grains [29]. Therefore, a fine-grain initial microstructure could also promote the heterogeneity in the stored energy field with shorter characteristic distances, and therefore higher tortuosity of the recrystallization front, and thus lead to higher twin densities.

## Conclusion

Two recrystallization experiment series were performed separately to analyze the influence of three thermo-mechanical processing parameters on annealing twin formation, i.e., the stored energy level and annealing temperature on one hand and the heating velocity on the other hand, leading to the following conclusions:

- For a given initial grain size, annealing twin density in the overall microstructure after the completion of recrystallization appears to be primarily influenced by the deformation level

- For a given strain level, smaller initial grain size leads to higher twin density.
- Different annealing twin quantification methods, including twin density, number of twin boundaries per grain, and twin boundary fraction, can lead to different twin content interpretations depending on whether the average grain size is constant or not.
- The annealing twin content, measured as the twin density or the number of twin boundaries per grain in grains of similar sizes, is higher in the samples with higher deformation level. Therefore, the prior deformation level is confirmed to be a promoting factor for annealing twin formation during recrystallization.
- In the considered ranges, the annealing temperature and the heating velocity did not show any obvious effect on annealing twin formation during recrystallization.
- The recrystallization front tortuosity, as measured at the mesoscale in EBSD maps, appears to be positively correlated with the annealing twin density at the end of recrystallization, consistently with the effect of grain boundary curvature proposed in a previous paper [12]. The latter point should be further confirmed by applying the proposed method to larger datasets (2D and 3D, and more thermo-mechanical conditions).

**Acknowledgements** This work was funded by the French National Research Agency (ANR project called FORMATING: ANR-11-NS09-001-01) and the Materials World Network of the US National Science Foundation under grant number DMR-1107986.

## References

1. Wantanabe T (1984) Grain boundary design and control. *Res Mech* 11:47–84
2. Kumar M, King WE, Schwartz AJ (2000) Modifications to the microstructural topology in F.C.C. materials through thermo-mechanical processing. *Acta Mater* 48:2081–2091
3. Randle V (2004) Twinning-related grain boundary engineering. *Acta Mater* 52:4067–4081
4. Carpenter H, Tamura S (1926) The formation of twinned metallic crystals. *Proc. R. Soc.* 113:161
5. Gleiter H (1969) The formation of annealing twins. *Acta Metall* 17:1421–1428
6. Pande CS, Imam MA, Rath BB (1990) Study of annealing twins in FCC metals and alloys. *Metall Trans A* 21:2891–2896
7. Mahajan S, Pande CS, Imam MA, Rath BB (1997) Formation of annealing twins in F.C.C. crystals. *Acta Mater* 45:2633–2638

8. Song KH, Chun YB, Hwang SK (2007) Direct observation of annealing twin formation in a Pb-base alloy. *Mater Sci Eng A* 454–455:629–636
9. Thomson CB, Randle V (1990) A study of twinning in nickel. *Scr Mater* 35:385–390
10. Lee S-L, Richards NL (2005) The effect of single-step low strain and annealing of nickel on grain boundary character. *Mater Sci Eng A* 30:81–87
11. Cahoon JR, Li Q, Richards NL (2009) Microstructural and processing factors influencing the formation of annealing twins. *Mater Sci Eng A* 526:56–61
12. Jin Y, Lin B, Bernacki M, Rohrer GS, Rollett AD, Bozzolo N (2014) Annealing twin development during recrystallization and grain growth in pure Nickel. *Mater Sci Eng A* 597:295–303
13. Romero RJ, Murr LE (1995) Torque-related lamellar carbide growth associated with annealing twin in 304 stainless steel. *Acta Metall Mater* 43:461–469
14. Li B, Tin S (2014) The role of deformation temperature and strain on grain boundary engineering of Inconel 600. *Mater Sci Eng A* 603:104–113
15. Wang W, Brisset F, Helbert AL, Solas D, Drouelle I, Mathon MH, Baudin T (2014) Influence of stored energy on twin formation during primary recrystallization. *Mater Sci Eng A* 1(589):112–118
16. Bair JL, Hatch SL, Field DP (2014) Formation of annealing twin boundaries in nickel. *Scr Mater* 81:52–55
17. Chen XP, Li LF, Sun HF, Wang LX, Liu Q (2015) Studies on the evolution of annealing twins during recrystallization and grain growth in highly rolled pure nickel. *Mater Sci Eng A* 622:108–113
18. Li Z, Zhang L, Sun N, Sun Y, Shan A (2014) Effects of prior deformation and annealing process on microstructure and annealing twin density in a nickel based alloy. *Mater Charact* 95:299–306
19. Randle V (2002) Sigma-boundary statistics by length and number. *Interface Sci* 10:271–277
20. Kumar M, King WE (2005) Universal features of grain boundary networks in FCC materials. *J Mater Sci* 40:847–852. doi:[10.1007/s10853-005-6500-9](https://doi.org/10.1007/s10853-005-6500-9)
21. Alvi MH, Cheong SW, Suni JP, Weiland H, Rollett AD (2008) Cube texture in hot-rolled aluminum alloy 1050 (AA1050)—nucleation and growth behavior. *Acta Mater* 56:3098–3108
22. Brandon DG (1969) The structure of high-angle grain boundaries. *Acta Metall* 14:1479–1484
23. Wang W, Lartigue-Korinek S, Brisset F, Helbert AL, Bourgon J, Baudin T (2015) Formation of annealing twins during primary recrystallization of two low stacking fault energy Ni-based alloys. *J Mater Sci* 50:2167–2177. doi:[10.1007/s10853-014-8780-4](https://doi.org/10.1007/s10853-014-8780-4)
24. Wang S, Holm EA, Suni J, Alvi MH, Kalu PN, Rollett AD (2011) Modeling the recrystallized grain size in single phase materials. *Acta Mater* 59:3872–3882
25. Maksimova EL, Robkin EI, Shvindelman LS, Straumal BB (1989) Phase transitions at grain boundaries in the presence of impurities. *Acta Metal* 37:1995–1998
26. Zhang H, Srolovitz DJ (2006) Characterization of atomic motion governing grain boundary migration. *Phys Rev B* 74:115404
27. Yan X, Zhang H (2010) On the atomistic mechanisms of grain boundary migration in [001] twist boundaries: molecular dynamics simulations. *Comput Mater Sci* 48:773–782
28. Zhang H, Srolovitz DJ, Douglas JF, Warren JA (2009) Grain boundaries exhibit the dynamics of glass-forming liquids. *PNAS* 106:7735–7740
29. Humphreys FJ (2004) Recrystallization and related annealing phenomena. M. Hatherly, Elsevier, Amsterdam
30. Epstein N (1989) On tortuosity and the tortuosity factor in flow and diffusion through porous media. *Chem Eng Sci* 44:777–779
31. Martorano MA, Fortes MA, Padilha AF (2006) The growth of protrusion at the boundary of a recrystallized grain. *Acta Mater* 54:2769–2776
32. Kumar M, Schwartz AJ, King WE (2002) Microstructural evolution during grain boundary engineering of low to medium stacking fault energy fcc materials. *Acta Mater* 50:2599–2612